A Novel Quadrotor With a 3-Axis Deformable Frame Using Tilting Motions of Parallel Link Modules Without Thrust Loss

Sakaguchi, Akinori
Research Institute of Advanced Electric Propulsion Aircrafts, Kyushu University

Yamamoto, Kaoru
Faculty of Information Science and Electrical Engineering, Kyushu University

https://hdl.handle.net/2324/7172336

出版情報：IEEE Robotics and Automation Letters. 7 (4), pp.9581-9588, 2022-10. Institute of Electrical Electronics Engineers (IEEE)
バージョン：

A Novel Quadrotor with a 3-axis Deformable Frame using Tilting Motions of Parallel Link Modules without Thrust Loss

Akinori Sakaguchi[1] and Kaoru Yamamoto[2]

***Abstract*—We propose a novel quadrotor with a 3-axis deformable frame using parallel link modules. By adding three servo motors to the frame, it has two configurations, namely, roll-pitch deformation mode and yaw deformation mode. In the roll-pitch deformation mode, it can tilt and fold the frame in the roll and pitch directions independently, which gives it 6 controllable degrees of freedom (CDOF). In the yaw deformation mode, it can contract the whole frame in the yaw direction. We propose a design method without thrust loss at any deformed state in both modes. In experiments, we show that it can fly stably even when deformed in both modes by the extended conventional control method. Furthermore, its applications are presented to demonstrate its high versatility.**

***Index Terms*—Aerial systems: mechanics and control, mechanism design, aerial systems: applications**

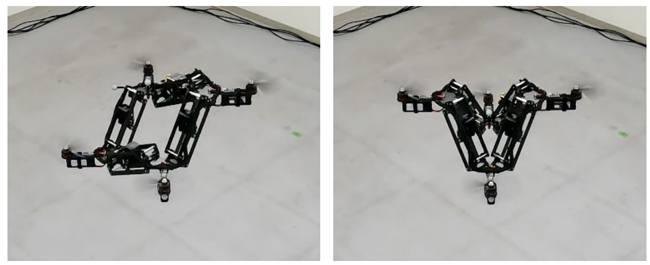

(a) roll-pitch deformation (b) yaw deformation

Fig. 1. Proposed quadrotor with a 3-axis deformable frame where figures (a) and (b) show the roll-pitch and yaw deformed states, respectively.

I. Introduction

A conventional multirotor has a simple structure in which multiple rotors are arranged on a fixed frame in the same plane and all their thrusts are parallel, so they can be used to cancel its gravity most efficiently in hovering [1]. However, since it has only 4 controllable degrees of freedom (CDOF), it cannot control its position and attitude independently.

To improve and enhance its capability, multirotors with tilting mechanisms using additional actuators have been attracting attention and have been proposed as shown in Table I, in which the number of additional actuators, the number of CDOF, its ability to deform in roll, pitch, and yaw directions, and its hovering efficiency are shown for each multirotor. In general, tiltable multirotors consume more energy in tilted states. Here, its hovering efficiency is marked ✓ if its hovering flight time t^{hover} is approximately equal to that of its non-tilted state, i.e., the state of a conventional multirotor $t^{\mathrm{hover}}_{\mathrm{conv}}$, and ✗ if $t^{\mathrm{hover}} < t^{\mathrm{hover}}_{\mathrm{conv}}$ clearly. The tilting mechanisms are mainly classified into four categories: tilting rotor [2]–[5], tilting arm [6]–[8], tilting link [9], [10], and tilting frame [11], [12]. Quadrotors with tilting rotors [2], [4] basically obtain a high CDOF by non-parallelizing the rotor thrusts at the expense of reduced flight time. A dual-axis tilting rotor [5] can gain 6 CDOF without reducing hovering efficiency by maintaining the parallelism of rotors, but the number of additional servo motors is large. A dual-axis tilting rotor with spherical-cylindrical composite joints [3] can gain 6 CDOF with only two servo motors while maintaining hovering efficiency. Quadrotors with tilting arms [6]–[8] can fold their arms in the yaw direction, but have only 4 CDOF and the overlapping of the rotors reduces hovering efficiency. A multirotor with tilting links [10] can deform the links in the roll, pitch, and yaw directions without loss of thrust using dual-axis gimbal modules, and has 6 CDOF, but it also requires a large number of additional servo motors. The deformation capability can perform many tasks such as transportation by grasping [8], [9], passing through narrow gaps [6], [8], and

TABLE I
Comparison of related work on tilting mechanisms.

Work	Additional actuators	CDOF	Deformation			Hovering efficiency
			roll	pitch	yaw	
[2]	2	5	✗	✗	✗	✗
[3]	2	6	✗	✗	✗	✓
[4]	4	6	✗	✗	✗	✗
[5]	8	6	✗	✗	✗	✓
[6], [7]	1	4	✗	✗	✓	✗
[8]	4	4	✗	✗	✓	✗
[9]	3	4	✗	✗	✓	✓
[10]	6	6	✓	✓	✓	✓
[11]	1	5	✗	✓	✗	✗
[12]	1	5	✗	✓	✗	✓
This work	3	6	✓	✓	✓	✓

Manuscript received: February, 24, 2022; Revised May, 30, 2022; Accepted June, 20, 2022.

This paper was recommended for publication by Editor Tamim Asfour upon evaluation of the Associate Editor and Reviewers' comments. This work was supported by JSPS KAKENHI Grant Numbers JP21K20406, JP19H02161, and JP20K14766.

[1]Akinori Sakaguchi is with the Research Institute of Advanced Electric Propulsion Aircrafts, Kyushu University, 744 Motooka, Nishi-ku, Fukuoka, Fukuoka, 819–0395, Japan `sakaguchi@ees.kyushu-u.ac.jp`

[2]Kaoru Yamamoto is with the Faculty of Information Science and Electrical Engineering, Kyushu University, 744 Motooka, Nishi-ku, Fukuoka, Fukuoka, 819–0395, Japan `yamamoto@ees.kyushu-u.ac.jp`

Digital Object Identifier (DOI): see top of this page.

manipulation [13], and can achieve high versatility. Therefore, the problem is *how to obtain both a high CDOF and a high deformation capability using as few additional actuators as possible without thrust loss*.

In this study, we consider a tilting frame incorporating the parallel link developed in our previous work [11], [12] as one module, and propose a novel quadrotor with a 3-axis deformable frame consisting of four modules connected in a string. The deformable frame enabled by combining tilting motions of the module with three servo motors can solve the problem mentioned above. As shown in Fig. 1, it has two deformation modes: a roll-pitch deformation mode that allows the frame to tilt and fold independently in the roll and pitch directions, giving it 6 CDOF, and a yaw deformation mode that allows the whole frame to contract in the yaw direction. At any deformed state in both modes, it can hover as efficiently as the conventional quadrotor.

The remainder of this paper is organized as follows. Section II describes the mechanism of the proposed deformable frame. Section III shows the design method without thrust loss. Section IV explains the control method extended from the conventional one. Section V shows the verification of the deformation capability by real experiments and its applications. Section VI gives the conclusion.

II. Mechanism

First, we explain the configuration of the proposed quadrotor. Then, the two deformation modes and their mechanism are described. Finally, we show the properties that hold for any deformed state in these two modes.

A. Deformable Frame using Parallel Link Modules

As shown in Fig. 2, the proposed quadrotor consists of four Y-shaped arms and four parallel link modules, which are connected to each other in a string of beads. Each arm has a rotor (a propeller, a motor, and an ESC). The parallel link module consists of upper and lower E-shaped tilting frames whose bearings as rotation fulcrums are embedded so that the frames form the parallel link mechanism. The module $i \in \{1, 2, 3, 4\}$ can tilt its frame around the $e_y^{\mathrm{m}i}$ axis of module i frame $\mathcal{F}^{\mathrm{m}i} = (\boldsymbol{e}_x^{\mathrm{m}i}, \boldsymbol{e}_y^{\mathrm{m}i}, \boldsymbol{e}_z^{\mathrm{m}i})$. Let $\theta^{\mathrm{m}i} \in \mathbb{R}$ be a tilt angle of module i that is defined by an angle between the $\boldsymbol{e}_x^{\mathrm{m}i}$ axis and the tilting frame. As a result of adopting the E-shape for the frame, the upper and lower frames do not interfere with each other when the module tilt angle is acute, and the range is $\theta^{\mathrm{m}i} \in [-\pi/2, \pi/2]$. As the module is tilted, its shape is deformed so that it is folded vertically according to the parallel link. The width $w^{\mathrm{m}}(\theta^{\mathrm{m}i})$ and height $h^{\mathrm{m}}(\theta^{\mathrm{m}i})$ of the skeleton model of the module, change as follows:

$$w^{\mathrm{m}}(\theta^{\mathrm{m}i}) = 2l^{\mathrm{f}} \cos(\theta^{\mathrm{m}i}),\ \ h^{\mathrm{m}}(\theta^{\mathrm{m}i}) = 2l^{\mathrm{f}} \left|\sin(\theta^{\mathrm{m}i})\right|, \quad (1)$$

where l^{f} is the tilting frame length. The important point is that the module maintains the parallel relation of the two arms connected to the module at any module tilt angle $\theta^{\mathrm{m}i}$, even if the shape is deformed as in equation (1).

Three of the parallel link modules 1, 2, and 3 have additional servo motors 1, 2, and 3, respectively, which are used to control the tilting motion of the module by directly driving the central rotation fulcrum of the upper frame. The module 4 has no servo motor. This structure creates two deformation modes, and in these modes, the quadrotor can deform into various shapes with three servo motors. The details of deformations are explained in the next subsection.

$$\theta^{\mathrm{m}1} = \theta^{\mathrm{m}3} = \theta^{\mathrm{pitch}},\ \theta^{\mathrm{m}2} = \theta^{\mathrm{m}4} = \theta^{\mathrm{roll}} \text{ if } \mathcal{M} = \mathcal{M}_{\text{roll-pitch}},$$
$$\theta^{\mathrm{m}1} = -\theta^{\mathrm{m}2} = -\theta^{\mathrm{m}3} = \theta^{\mathrm{m}4} = \theta^{\mathrm{yaw}} \text{ if } \mathcal{M} = \mathcal{M}_{\mathrm{yaw}}.$$

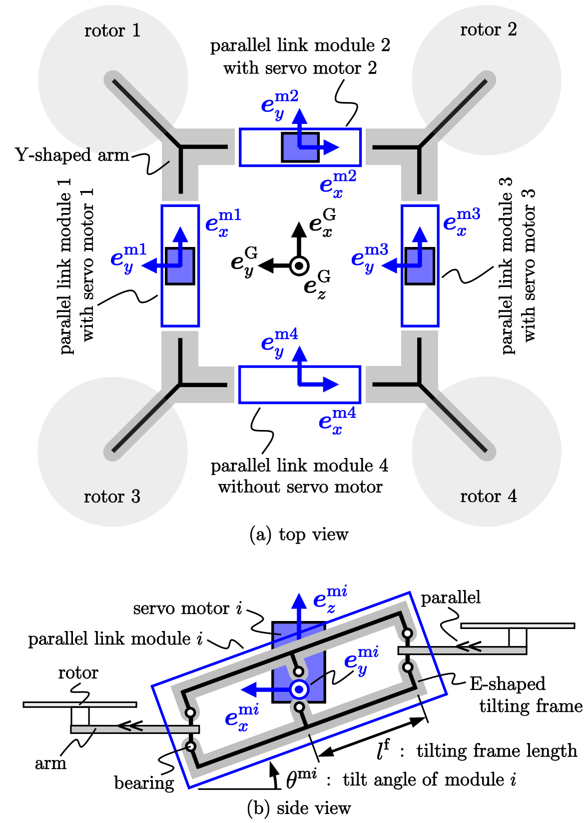

Fig. 2. Mechanical model of the proposed quadrotor.

B. Two Deformation Modes

The quadrotor with the deformable frame has two deformation modes $\mathcal{M} \in \{\mathcal{M}_{\text{roll-pitch}}, \mathcal{M}_{\mathrm{yaw}}\}$: roll-pitch deformation mode $\mathcal{M}_{\text{roll-pitch}}$ and yaw deformation mode $\mathcal{M}_{\mathrm{yaw}}$. The transitions of the two modes are shown in Fig. 3. The modes are switched through the conventional quadrotor state at $\theta^{\mathrm{m}1} = \theta^{\mathrm{m}2} = \theta^{\mathrm{m}3} = \theta^{\mathrm{m}4} = 0$, since in each mode the tilt

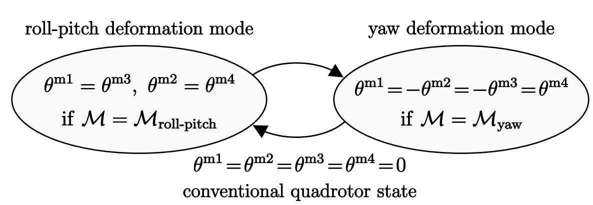

Fig. 3. Transitions of deformation modes.

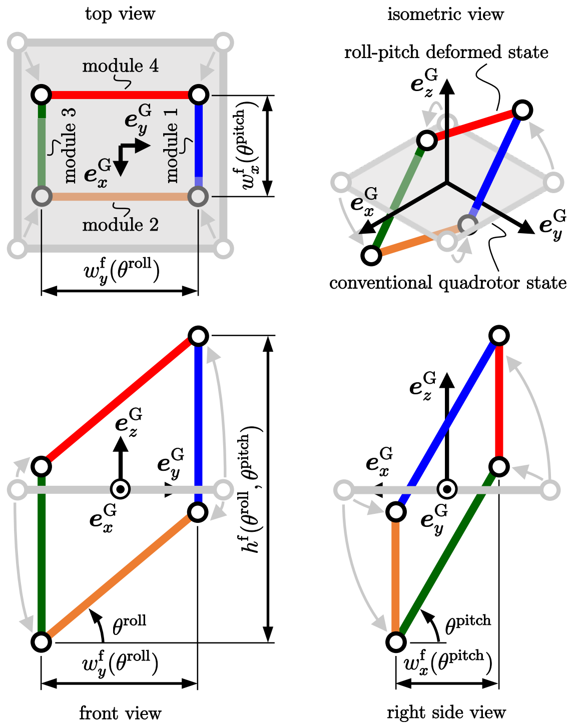

Fig. 4. A simple skeleton model of the roll-pitch deformed state in Fig. 1 (a) from the conventional quadrotor state.

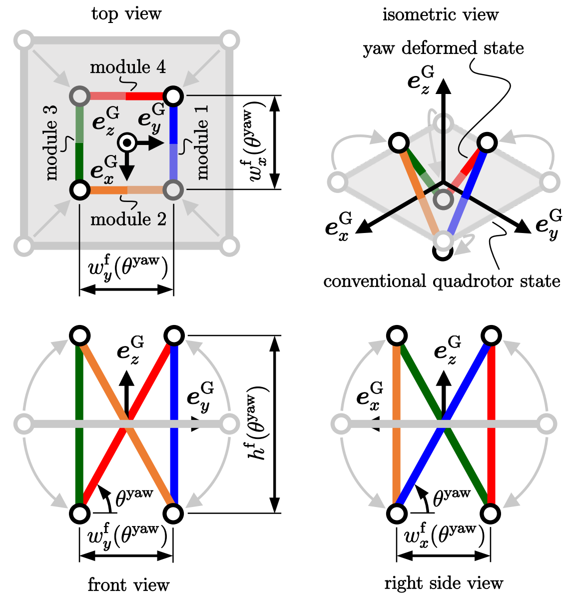

Fig. 5. A simple skeleton model of the yaw deformed state in Fig. 1 (b) from the conventional quadrotor state.

angles of the modules are constrained as follows:

$$\theta^{\mathrm{m1}} = \theta^{\mathrm{m3}},\ \theta^{\mathrm{m2}} = \theta^{\mathrm{m4}} \text{ if } \mathcal{M} = \mathcal{M}_{\text{roll-pitch}}, \tag{2}$$

$$\theta^{\mathrm{m1}} = -\theta^{\mathrm{m2}} = -\theta^{\mathrm{m3}} = \theta^{\mathrm{m4}} \text{ if } \mathcal{M} = \mathcal{M}_{\mathrm{yaw}}. \tag{3}$$

From the above equations, the module tilt angles are represented by two parameters $\theta^{\mathrm{roll}}, \theta^{\mathrm{pitch}} \in [-\pi/2, \pi/2]$ in $\mathcal{M}_{\text{roll-pitch}}$ and parameter $\theta^{\mathrm{yaw}} \in [-\pi/2, \pi/2]$ in $\mathcal{M}_{\mathrm{yaw}}$. The three parameters are collectively referred to as $\boldsymbol{\theta}^{\mathrm{rpy}} = [\theta^{\mathrm{roll}}\ \theta^{\mathrm{pitch}}\ \theta^{\mathrm{yaw}}]^{\top}$. Thus, equations (2) and (3) can be rewritten as follows:

$$\boldsymbol{\theta}^{\mathrm{m}} = \begin{cases} [\theta^{\mathrm{pitch}}\ \theta^{\mathrm{roll}}\ \theta^{\mathrm{pitch}}\ \theta^{\mathrm{roll}}]^{\top} \text{ if } \mathcal{M} = \mathcal{M}_{\text{roll-pitch}}, \\ [\theta^{\mathrm{yaw}}\ -\theta^{\mathrm{yaw}}\ -\theta^{\mathrm{yaw}}\ \theta^{\mathrm{yaw}}]^{\top} \text{ if } \mathcal{M} = \mathcal{M}_{\mathrm{yaw}}, \end{cases} \tag{4}$$

where $\boldsymbol{\theta}^{\mathrm{m}} = [\theta^{\mathrm{m1}}\ \theta^{\mathrm{m2}}\ \theta^{\mathrm{m3}}\ \theta^{\mathrm{m4}}]^{\top}$ are the tilt angles of the modules. The details of the deformations characterized by parameters θ^{roll}, θ^{pitch}, and θ^{yaw} are described below.

Next, using the simplified skeleton models shown in Figs. 4 and 5 where the modules are the links and the arms are the joints, we explain the mechanism of deformations in the roll, pitch, and yaw directions around the e_x^{G}, e_y^{G}, and e_z^{G} axes of the geometric frame $\mathcal{F}^{\mathrm{G}} = (\boldsymbol{e}_x^{\mathrm{G}}, \boldsymbol{e}_y^{\mathrm{G}}, \boldsymbol{e}_z^{\mathrm{G}})$ with the geometric center $\boldsymbol{p}^{\mathrm{G}}$ at the origin, respectively. Fig. 4 shows a simple skeleton model of the roll-pitch deformed state. The four modules form a rhombus with side lengths $2l^{\mathrm{f}}$. Thus, the facing modules are parallel and their tilting motions are interlocked as in (4): modules 1 and 3 tilt by θ^{pitch} around the e_y^{G} axis, and modules 2 and 4 tilt by θ^{roll} around the e_x^{G} axis. Since the tilting motions of modules 1 and 3 are independent of those of modules 2 and 4, various rhombuses are formed with the tilting motions depending on the parameters θ^{roll} and θ^{pitch}. The widths w_x^{f}, w_y^{f}, and height h^{f} of the deformable frame change in e_x^{G}, e_y^{G}, and e_z^{G}, respectively, as follows:

$$\begin{aligned} &w_x^{\mathrm{f}} = w^{\mathrm{m}}(\theta^{\mathrm{pitch}}),\ w_y^{\mathrm{f}} = w^{\mathrm{m}}(\theta^{\mathrm{roll}}), \\ &h^{\mathrm{f}} = h^{\mathrm{m}}(\theta^{\mathrm{roll}}) + h^{\mathrm{m}}(\theta^{\mathrm{pitch}}) \text{ if } \mathcal{M} = \mathcal{M}_{\text{roll-pitch}}. \end{aligned} \tag{5}$$

The widths w_x^{f} and w_y^{f} decrease depending on θ^{pitch} and θ^{roll}, respectively, while the height h^{f} increases depending on both θ^{roll} and θ^{pitch}, so the roll-pitch deformed frame becomes vertically elongated up to the maximum height $4l^{\mathrm{f}}$ at $\theta^{\mathrm{roll}} = \theta^{\mathrm{pitch}} = \pm\pi/2$. Fig. 5 shows a simple skeleton model of the yaw deformed state. The four modules form V-shapes and inverted V-shapes with the neighboring modules. For example, module 1 forms a V-shape with module 2 and an inverted V-shape with module 4. As the angles of the tips of the V-shapes and inverted V-shapes decrease due to the opposing tilting motions of the facing modules, the frame shape is contracted in the yaw direction around the e_z^{G} axis. When contracting, the widths w_x^{f}, w_y^{f}, and height h^{f} of the deformable frame change as follows:

$$\begin{aligned} &w_x^{\mathrm{f}} = w_y^{\mathrm{f}} = w^{\mathrm{m}}(\theta^{\mathrm{yaw}}), \\ &h^{\mathrm{f}} = h^{\mathrm{m}}(\theta^{\mathrm{yaw}}) \text{ if } \mathcal{M} = \mathcal{M}_{\mathrm{yaw}}. \end{aligned} \tag{6}$$

Depending on θ^{yaw}, both widths w_x^{f} and w_y^{f} decrease equally, while the height h^{f} increases up to $2l^{\mathrm{f}}$ at $\theta^{\mathrm{yaw}} = \pm\pi/2$. In summary, in $\mathcal{M}_{\text{roll-pitch}}$, the proposed quadrotor can tilt its frame independently in the roll and pitch directions, and the frame is folded vertically. In $\mathcal{M}_{\mathrm{yaw}}$, it cannot tilt its frame in the yaw direction, but it can contract its shape in the yaw direction. To perform the roll-pitch and yaw deformations shown in Figs. 4 and 5, additional servo motors to drive the tilt angles $\boldsymbol{\theta}^{\mathrm{m}}$ of the modules as in (4) are required for modules 1 and 2 in $\mathcal{M}_{\text{roll-pitch}}$, and for modules 1 and 3 in $\mathcal{M}_{\mathrm{yaw}}$.

Therefore, to achieve both modes, only three servo motors need to be added to modules 1, 2, and 3, as shown in Fig. 2.

Finally, it has the following two properties, which hold in both modes $\mathcal{M}_{\text{roll-pitch}}$ and $\mathcal{M}_{\text{yaw}}$.

Property 1: With the parallel link modules, all rotor planes are always parallel at any deformed state, that is, $^\forall\mathcal{M} \in \{\mathcal{M}_{\text{roll-pitch}}, \mathcal{M}_{\text{yaw}}\},\ ^\forall\theta^{\text{m}i},\ i \in \{1,2,3,4\}$,

$$\boldsymbol{f}^{\text{r}1} \parallel \boldsymbol{f}^{\text{r}2} \parallel \boldsymbol{f}^{\text{r}3} \parallel \boldsymbol{f}^{\text{r}4}, \tag{7}$$

where $\boldsymbol{f}^{\text{r}i}$ is the thrust vector of rotor i. This indicates that the same property as the conventional quadrotor is preserved.

Property 2: In any deformed state, the airframe shape is symmetric with respect to the geometric frame $\mathcal{F}^{\text{G}}$, that is, $^\forall\mathcal{M} \in \{\mathcal{M}_{\text{roll-pitch}}, \mathcal{M}_{\text{yaw}}\},\ ^\forall\theta^{\text{m}i},\ i \in \{1,2,3,4\}$,

$$\boldsymbol{p}^{\text{m}1} = -\boldsymbol{p}^{\text{m}3},\ \boldsymbol{p}^{\text{m}2} = -\boldsymbol{p}^{\text{m}4}, \tag{8}$$

$$\boldsymbol{p}^{\text{a}1}_{xy} = -\boldsymbol{p}^{\text{a}3}_{xy},\ \boldsymbol{p}^{\text{a}2}_{xy} = -\boldsymbol{p}^{\text{a}4}_{xy},\ \sum_{i=1}^{4} p^{\text{a}i}_z = 0, \tag{9}$$

where $\boldsymbol{p}^{\text{m}i}$ and $\boldsymbol{p}^{\text{a}i} = [(\boldsymbol{p}^{\text{a}i}_{xy})^\top\ p^{\text{a}i}_z]^\top$ are the center of gravity (CoG) positions of module i and arm i in $\mathcal{F}^{\text{G}}$, respectively.

III. Design without Rotor Thrust Loss due to Deformations

In quadrotors with tilting mechanisms, hovering inefficiencies occurs mainly due to the following three cases.

Case 1: The rotor thrust vectors $\boldsymbol{f}^{\text{r}i}$ become non-parallel, that is, for $i, j \in \{1,2,3,4\},\ i \neq j$,

$$\boldsymbol{f}^{\text{r}i} \nparallel \boldsymbol{f}^{\text{r}j}. \tag{10}$$

This occurs in a quadrotor with tilting rotors [4].

Case 2: The overlap among rotors and the overlap between rotors and other parts reduce the thrust of the rotor, which occurs in the O-shaped state of a quadrotor with tilting arms [8].

Case 3: The rotor configuration is asymmetric about either the $\boldsymbol{e}^{\text{CoG}}_x$ or $\boldsymbol{e}^{\text{CoG}}_y$ axis of the CoG frame $\mathcal{F}^{\text{CoG}} = (\boldsymbol{e}^{\text{CoG}}_x, \boldsymbol{e}^{\text{CoG}}_y, \boldsymbol{e}^{\text{CoG}}_z)$, or both axes, which occurs in the T-shaped state of the tilting arms [8].

In this section, we show how to design the proposed airframe so that all the cases (*Cases 1*, *2*, and *3*) are avoided at any deformed state. This means that the proposed quadrotor can fly as efficiently as the conventional one in the hovering state.

First, from *Property 1*, *Case 1* does not occur at any deformation state in both modes $\mathcal{M}_{\text{roll-pitch}}$ and $\mathcal{M}_{\text{yaw}}$.

Next, we derive a condition for the Y-shaped arm length $l^{\text{a}} = \sum_{i=1}^{3} l^{\text{a}}_i$ that does not cause *Case 2*. The arm lengths $l^{\text{a}}_1, l^{\text{a}}_2, l^{\text{a}}_3$ are shown in Fig. 6. Since all the rotors and all the arms are parallel from *Property 1*, we consider the overlap of the rotor and arm projections onto the $\boldsymbol{e}^{\text{G}}_x$-$\boldsymbol{e}^{\text{G}}_y$ plane of the geometric frame $\mathcal{F}^{\text{G}}$. If the rotors do not overlap at $w^{\text{m}}(\pm\pi/2) = 0$ for all module widths where $\theta^{\text{pitch}} = \theta^{\text{roll}} = \pm\pi/2$ in $\mathcal{M}_{\text{roll-pitch}}$ or $\theta^{\text{yaw}} = \pm\pi/2$ in $\mathcal{M}_{\text{yaw}}$, overlapping of all rotors can be avoided at any deformation state. The condition is given by $l^{\text{a}}_1 + l^{\text{a}}_2 + l^{\text{a}}_3 \geq l^{\text{r}}$ where l^{r} is the rotor radius and $l^{\text{a}}_1, l^{\text{a}}_2, l^{\text{a}}_3$ are arm lengths. Here, l^{a}_1 and l^{a}_2 are automatically determined by the tilting frame length and servo motor width, respectively. Also, the condition that the rotor plane does not overlap the 90-degree bifurcated plane of the Y-shaped arm is given by $\sqrt{2} l^{\text{a}}_3 \geq l^{\text{r}}$. Therefore, to avoid *Case 2*, the arm length l^{a}_3 should be extended so that the following condition is satisfied:

$$l^{\text{a}}_3 \geq \max\left\{ l^{\text{r}} - l^{\text{a}}_1 - l^{\text{a}}_2,\ l^{\text{r}}/\sqrt{2} \right\}. \tag{11}$$

Finally, we derive a mass condition that avoids *Case 3*, and show component arrangements that satisfy it. Since the rotor configuration is symmetric with respect to the $\boldsymbol{e}^{\text{G}}_x$ and $\boldsymbol{e}^{\text{G}}_y$ axes of $\mathcal{F}^{\text{G}}$ from *Property 2*, we derive the condition that the center of gravity $\boldsymbol{p}^{\text{CoG}}_{xy}$ is equal to the geometric center $\boldsymbol{p}^{\text{G}}_{xy}$, i.e., $\boldsymbol{p}^{\text{CoG}}_{xy} = \boldsymbol{p}^{\text{G}}_{xy}$. The error $\boldsymbol{p}^{\Delta}$ of these vectors is represented as

$$\boldsymbol{p}^{\Delta} = \frac{\sum_{i=1}^{4} \left(m^{\text{m}i}\boldsymbol{p}^{\text{m}i} + m^{\text{a}i}\boldsymbol{p}^{\text{a}i} \right)}{m}, \tag{12}$$

where $\boldsymbol{p}^{\text{m}i}$ and $\boldsymbol{p}^{\text{a}i}$ are the CoG positions of module i and arm i in $\mathcal{F}^{\text{G}}$, respectively. $m = \sum_{i=1}^{4}(m^{\text{m}i} + m^{\text{a}i})$ is the total mass of all components where $m^{\text{m}i}$ and $m^{\text{a}i}$ are the masses of module i and arm i, respectively. From (12) using *Property 2*, the sufficient conditions for the masses of modules and arms such that $\boldsymbol{p}^{\Delta}_{xy} = \boldsymbol{0}$ or $\boldsymbol{p}^{\Delta} = \boldsymbol{0}$, are as follows:

$$\begin{aligned} &m^{\text{m}1} = m^{\text{m}3},\ m^{\text{m}2} = m^{\text{m}4}, \\ &\qquad m^{\text{a}1} = m^{\text{a}3},\ m^{\text{a}2} = m^{\text{a}4} \text{ for } \boldsymbol{p}^{\Delta}_{xy} = \boldsymbol{0}, \end{aligned} \tag{13}$$

$$\begin{aligned} &m^{\text{m}1} = m^{\text{m}3},\ m^{\text{m}2} = m^{\text{m}4}, \\ &\qquad m^{\text{a}1} = m^{\text{a}2} = m^{\text{a}3} = m^{\text{a}4} \text{ for } \boldsymbol{p}^{\Delta} = \boldsymbol{0}. \end{aligned} \tag{14}$$

If the condition (14) holds, the CoG $\boldsymbol{p}^{\text{CoG}}$ will not change in e^{G}_x, e^{G}_y, and e^{G}_z due to deformations in addition to avoiding *Case 3*. Here, we must arrange the components (battery, flight computer, and companion computer) in the modules, arms, or both, such that the mass condition (13) or (14) is satisfied. However, since the ratio of the battery mass to the airframe mass is relatively large in order to extend the flight time, arranging a single battery in the module or arm will result in non-uniform mass distribution, and it is difficult to satisfy equation (13) or (14). To solve this problem, by distributing $n^{\text{b}}(= 2,4,6,8)$ identical batteries as shown in Fig. 7, the batteries can be arranged regardless of their capacity while

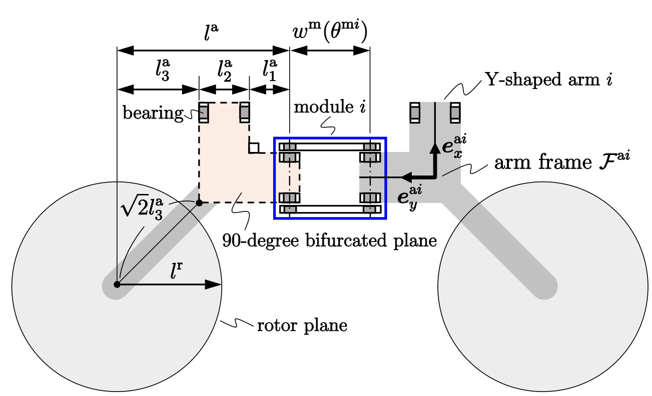

Fig. 6. Arm lengths $l^{\text{a}}_1, l^{\text{a}}_2, l^{\text{a}}_3$.

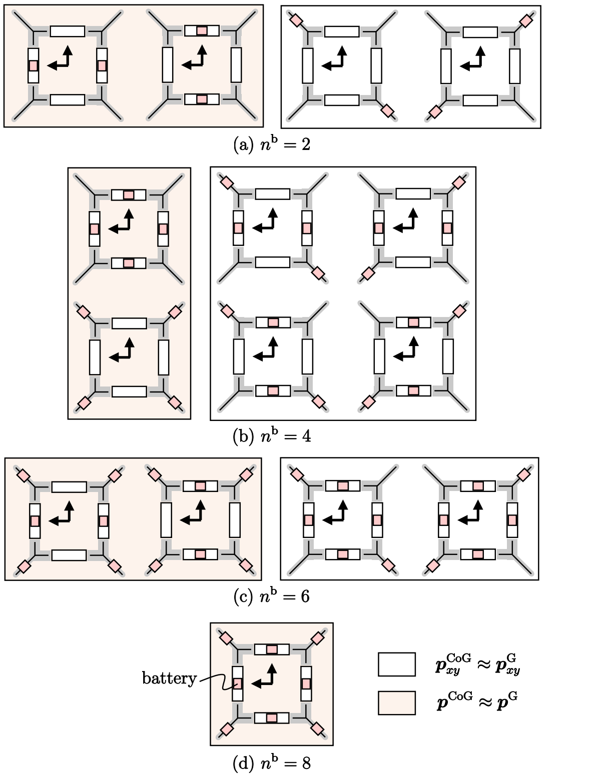

Fig. 7. Arrangement of n^{b} batteries such that $\boldsymbol{p}^{\mathrm{CoG}}_{xy} \approx \boldsymbol{p}^{\mathrm{G}}_{xy}$ or $\boldsymbol{p}^{\mathrm{CoG}} \approx \boldsymbol{p}^{\mathrm{G}}$.

trying to satisfy (13) and (14). However, only module 4 does not have an additional servo motor, hence $m^{\mathrm{m1}} = m^{\mathrm{m3}}$ and $m^{\mathrm{m2}} \neq m^{\mathrm{m4}}$. The xy error $\boldsymbol{p}^{\Delta}_{xy}$ of (12) at $m^{\mathrm{m2}} \neq m^{\mathrm{m4}}$ is given by the following equation:

$$\boldsymbol{p}^{\Delta}_{xy} = \frac{m^{\Delta}}{m}\boldsymbol{p}^{\mathrm{m4}}_{xy} = \frac{m^{\Delta}}{m}\begin{bmatrix} -l^{\mathrm{f}}\cos(\theta^{\mathrm{m1}}) - l^{\mathrm{a}}_1 - l^{\mathrm{a}}_2/2 \\ 0 \end{bmatrix}, \tag{15}$$

where $m^{\Delta} = m^{\mathrm{m4}} - m^{\mathrm{m2}}$ is the mass difference between modules 2 and 4. If the mass ratio m^{Δ}/m is approximately equal to 0, then $\boldsymbol{p}^{\Delta}_{xy} \approx \mathbf{0}$. Therefore, the two computers should be selected and mounted in modules 2 and 4 in order to get $m^{\Delta}/m \approx 0$. Also, the position $\boldsymbol{p}^{\mathrm{m4}}_{xy}$ of module 4 depends on θ^{m1}, and the more the quadrotor is deformed, the less it is affected by the discrepancy $\boldsymbol{p}^{\Delta}_{xy}$ between the CoG and the geometric center.

In the following, we summarize the design procedure.

1) The arm lengths l^{a}_1, l^{a}_2, and rotor radius l^{r} are given by the tilting frame length, servo motor width, and propeller radius, respectively, and the arm length l^{a}_3 is determined by (11).
2) For the given number $n^{\mathrm{b}}(=2,4,6,8)$ of identical batteries with option $\boldsymbol{p}^{\Delta}_{xy} \approx \mathbf{0}$ or $\boldsymbol{p}^{\Delta} \approx \mathbf{0}$ for the CoG, the battery arrangement is determined from Fig. 7.
3) Two computers (flight computer and companion computer) are selected and mounted in modules 2 and 4 so that $m^{\Delta}/m \approx 0$.

IV. Control

We describe a control architecture of the proposed quadrotor as shown in Fig. 8 under three assumptions: (i) it behaves as a single rigid body, (ii) its CoG coincides with its geometric center, and (iii) all rotor planes are parallel to the mounting plane of the flight computer. Assumptions (i), (ii), and (iii) are satisfied by slow deformations in hovering, by the design in Section III, and by the parallel link modules, respectively. Note that assumption (i) may be violated by rotor turbulence. However, by Section III, it is designed not to be affected by rotor turbulence at any deformed state in hovering. In addition, under the condition of slow deformation while hovering, the external forces acting on the module, such as anti-torque by tilting and control torque by rotors, are negligible and its backdrivability is low. Therefore, assumption (i) still holds even if rotor turbulence is present.

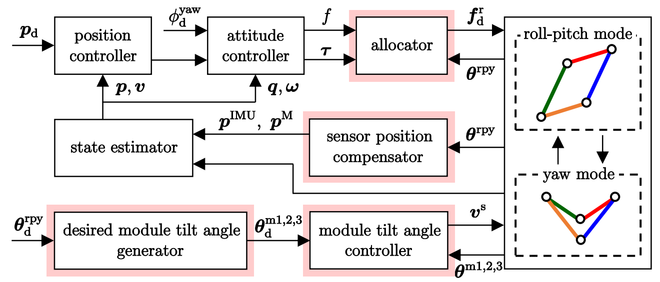

Fig. 8. Control architecture that extends conventional control method where the red blocks are the extended components.

First, we briefly explain its position and attitude control to achieve stabilization at a given desired position $\boldsymbol{p}_{\mathrm{d}}$ and yaw angle $\phi^{\mathrm{yaw}}_{\mathrm{d}}$. Under the above assumptions, its flight principle is the same as that of conventional quadrotors, and their standard control methods, such as a cascaded PID controller and a Mellinger controller, can be applied to the position and attitude controllers shown in Fig. 8. Here, we use a cascaded position and velocity PID controller and a cascaded attitude and angular velocity PID controller, which are employed in the open-source flight control software `PX4` [14]. These controllers generate the total thrust f along the $\boldsymbol{e}^{\mathrm{CoG}}_z$ axis and torque $\boldsymbol{\tau}$ about the $\boldsymbol{e}^{\mathrm{CoG}}_x$, $\boldsymbol{e}^{\mathrm{CoG}}_y$, and $\boldsymbol{e}^{\mathrm{CoG}}_z$ axes. From the following equation, the allocator converts the control inputs f and $\boldsymbol{\tau}$ into the desired rotor thrusts $\boldsymbol{f}^{\mathrm{r}}_{\mathrm{d}} = [f^{\mathrm{r1}}_{\mathrm{d}}\ f^{\mathrm{r2}}_{\mathrm{d}}\ f^{\mathrm{r3}}_{\mathrm{d}}\ f^{\mathrm{r4}}_{\mathrm{d}}]^{\top}$, where $f^{\mathrm{r}i}_{\mathrm{d}}$ is the desired rotor thrust of rotor i.

$$\begin{bmatrix} f \\ \boldsymbol{\tau} \end{bmatrix} = T(\boldsymbol{\theta}^{\mathrm{rpy}})\boldsymbol{f}^{\mathrm{r}}_{\mathrm{d}}, \tag{16}$$

where $T(\boldsymbol{\theta}^{\mathrm{rpy}})$ is the following matrix whose elements are the length $l(\cdot) = l^{\mathrm{f}}\cos(\cdot) + l^{\mathrm{a}}$ between the CoG and the rotor, and rotor specific anti-torque constant κ:

$$T(\boldsymbol{\theta}^{\mathrm{rpy}}) = \begin{cases} \begin{bmatrix} 1 & 1 & 1 & 1 \\ l(\theta^{\mathrm{roll}}) & -l(\theta^{\mathrm{roll}}) & l(\theta^{\mathrm{roll}}) & -l(\theta^{\mathrm{roll}}) \\ -l(\theta^{\mathrm{pitch}}) & -l(\theta^{\mathrm{pitch}}) & l(\theta^{\mathrm{pitch}}) & l(\theta^{\mathrm{pitch}}) \\ \kappa & -\kappa & -\kappa & \kappa \end{bmatrix} & \text{if } \mathcal{M} = \mathcal{M}_{\text{roll-pitch}}, \\ \begin{bmatrix} 1 & 1 & 1 & 1 \\ l(\theta^{\mathrm{yaw}}) & -l(\theta^{\mathrm{yaw}}) & l(\theta^{\mathrm{yaw}}) & -l(\theta^{\mathrm{yaw}}) \\ -l(\theta^{\mathrm{yaw}}) & -l(\theta^{\mathrm{yaw}}) & l(\theta^{\mathrm{yaw}}) & l(\theta^{\mathrm{yaw}}) \\ \kappa & -\kappa & -\kappa & \kappa \end{bmatrix} & \text{if } \mathcal{M} = \mathcal{M}_{\text{yaw}}. \end{cases} \tag{17}$$

The matrix $T(\boldsymbol{\theta}^{\mathrm{rpy}})$ depends on θ^{roll}, θ^{pitch}, and θ^{yaw}, but it is always invertible. Therefore, it does not have the singularity that the roll, pitch, or yaw control torque becomes 0 at a specific deformed state, which occurs in quadrotors with tilting mechanisms [6], [7], [11].

Next, we explain the tilt control of the modules with the servo motors. The desired module tilt angle generator outputs the desired value $\boldsymbol{\theta}_{\mathrm{d}}^{\mathrm{m}1,2,3} = [\theta_{\mathrm{d}}^{\mathrm{m}1}\ \theta_{\mathrm{d}}^{\mathrm{m}2}\ \theta_{\mathrm{d}}^{\mathrm{m}3}]^{\top}$ for tilt angles of modules 1, 2, and 3 as follows:

$$\boldsymbol{\theta}_{\mathrm{d}}^{\mathrm{m}1,2,3} = \begin{bmatrix} 0 & 1 & 1 \\ 1 & 0 & -1 \\ 0 & 1 & -1 \end{bmatrix} \boldsymbol{\theta}_{\mathrm{d}}^{\mathrm{rpy}}. \tag{18}$$

Note that the desired value $\boldsymbol{\theta}_{\mathrm{d}}^{\mathrm{rpy}} = [\theta_{\mathrm{d}}^{\mathrm{roll}}\ \theta_{\mathrm{d}}^{\mathrm{pitch}}\ \theta_{\mathrm{d}}^{\mathrm{yaw}}]^{\top}$ for the deformation parameter $\boldsymbol{\theta}^{\mathrm{rpy}}$ is given by

$$\boldsymbol{\theta}_{\mathrm{d}}^{\mathrm{rpy}} = \begin{cases} [\theta_{\mathrm{d}}^{\mathrm{roll}}\ \theta_{\mathrm{d}}^{\mathrm{pitch}}\ 0]^{\top} \text{ if } \mathcal{M} = \mathcal{M}_{\text{roll-pitch}}, \\ [0\ 0\ \theta_{\mathrm{d}}^{\mathrm{yaw}}]^{\top} \text{ if } \mathcal{M} = \mathcal{M}_{\mathrm{yaw}}. \end{cases} \tag{19}$$

The module tilt angle controller outputs the voltage $\boldsymbol{v}^{\mathrm{s}}$ for servo motors 1, 2, and 3 as $\boldsymbol{v}^{\mathrm{s}} = \boldsymbol{K}_{\mathrm{p}}^{\mathrm{m}1,2,3}(\boldsymbol{\theta}_{\mathrm{d}}^{\mathrm{m}1,2,3} - \boldsymbol{\theta}^{\mathrm{m}1,2,3})$, where $\boldsymbol{K}_{\mathrm{p}}^{\mathrm{m}1,2,3}$ is the gain matrix and $\boldsymbol{\theta}^{\mathrm{m}1,2,3} = [\theta^{\mathrm{m}1}\ \theta^{\mathrm{m}2}\ \theta^{\mathrm{m}3}]^{\top}$ are the tilt agnles of modules 1, 2, and 3. Note that the tilt angles $\theta^{\mathrm{m}i}$ of the modules 1, 2, and 3 are equal to the angles $\theta^{\mathrm{s}i}$ of the servo motors 1, 2, and 3, respectively, i.e., $\theta^{\mathrm{m}i} = \theta^{\mathrm{s}i}$ for $i = 1, 2, 3$.

Finally, we describe the position compensation of sensors such as IMU (3-axis accelerometer, 3-axis gyroscope, and 3-axis magnetometer) and GPS in the outdoor case (reflective markers of motion capture system in the indoor case) for the state estimator. The flight computer with the IMU is mounted in module 4. Since the experiments in the next section use a motion capture system, markers are mounted on arm 4 in this study. In this case, the sensor position compensator modifies the IMU position $\boldsymbol{p}^{\mathrm{IMU}}$ and marker position $\boldsymbol{p}^{\mathrm{M}}$ in the CoG frame $\mathcal{F}^{\mathrm{CoG}}$ according to the deformations as follows:

$$\boldsymbol{p}^{\mathrm{IMU}} = \boldsymbol{p}^{\mathrm{m}4} + \boldsymbol{p}_{\mathrm{offset}}^{\mathrm{IMU}},\ \boldsymbol{p}^{\mathrm{M}} = \boldsymbol{p}^{\mathrm{a}4} + \boldsymbol{p}_{\mathrm{offset}}^{\mathrm{M}}, \tag{20}$$

where $\boldsymbol{p}_{\mathrm{offset}}^{\mathrm{IMU}}$ and $\boldsymbol{p}_{\mathrm{offset}}^{\mathrm{M}}$ are the CoG positions of the IMU and markers in $\mathcal{F}^{\mathrm{m}4}$ and $\mathcal{F}^{\mathrm{a}4}$, respectively. $\boldsymbol{p}^{\mathrm{m}4}$ and $\boldsymbol{p}^{\mathrm{a}4}$ are the following CoG positions of module 4 and arm 4, respectively.

$$\boldsymbol{p}^{\mathrm{m}4} = \begin{cases} \begin{bmatrix} -l^{\mathrm{f}}\cos(\theta^{\mathrm{pitch}}) - l_1^{\mathrm{a}} - l_2^{\mathrm{a}}/2 \\ 0 \\ l^{\mathrm{f}}\sin(\theta^{\mathrm{pitch}}) \end{bmatrix} \text{ if } \mathcal{M} = \mathcal{M}_{\text{roll-pitch}}, \\ \begin{bmatrix} -l^{\mathrm{f}}\cos(\theta^{\mathrm{yaw}}) - l_1^{\mathrm{a}} - l_2^{\mathrm{a}}/2 \\ \mathbf{0} \end{bmatrix} \text{ if } \mathcal{M} = \mathcal{M}_{\mathrm{yaw}}, \end{cases} \tag{21}$$

$$\boldsymbol{p}^{\mathrm{a}4} = \begin{cases} \begin{bmatrix} -l^{\mathrm{f}}\cos(\theta^{\mathrm{pitch}}) - l_1^{\mathrm{a}} - l_2^{\mathrm{a}}/2 \\ -l^{\mathrm{f}}\cos(\theta^{\mathrm{roll}}) - l_1^{\mathrm{a}} - l_2^{\mathrm{a}}/2 \\ -l^{\mathrm{f}}\sin(\theta^{\mathrm{roll}}) + l^{\mathrm{f}}\sin(\theta^{\mathrm{pitch}}) \end{bmatrix} \text{ if } \mathcal{M} = \mathcal{M}_{\text{roll-pitch}}, \\ \begin{bmatrix} -l^{\mathrm{f}}\cos(\theta^{\mathrm{yaw}}) - l_1^{\mathrm{a}} - l_2^{\mathrm{a}}/2 \\ -l^{\mathrm{f}}\cos(\theta^{\mathrm{yaw}}) - l_1^{\mathrm{a}} - l_2^{\mathrm{a}}/2 \\ -l^{\mathrm{f}}\sin(\theta^{\mathrm{yaw}}) \end{bmatrix} \text{ if } \mathcal{M} = \mathcal{M}_{\mathrm{yaw}}. \end{cases} \tag{22}$$

Based on the compensated positions $\boldsymbol{p}^{\mathrm{IMU}}$ and $\boldsymbol{p}^{\mathrm{M}}$, the state estimator feeds back the estimated state (position $\boldsymbol{p}$, velocity $\boldsymbol{v}$, quaternion $\boldsymbol{q}$, and anguler velocity $\boldsymbol{\omega}$) to the position and attitude controllers using an extended Kalman filter.

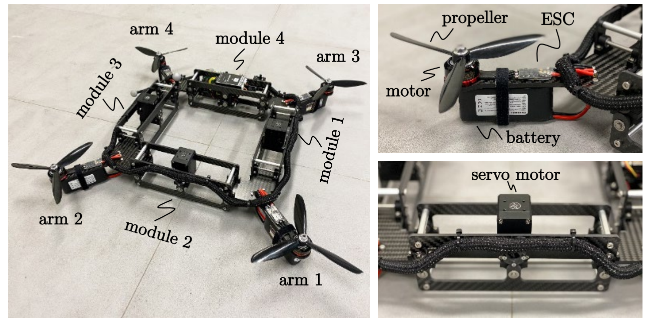

Fig. 9. Prototype of the proposed quadrotor.

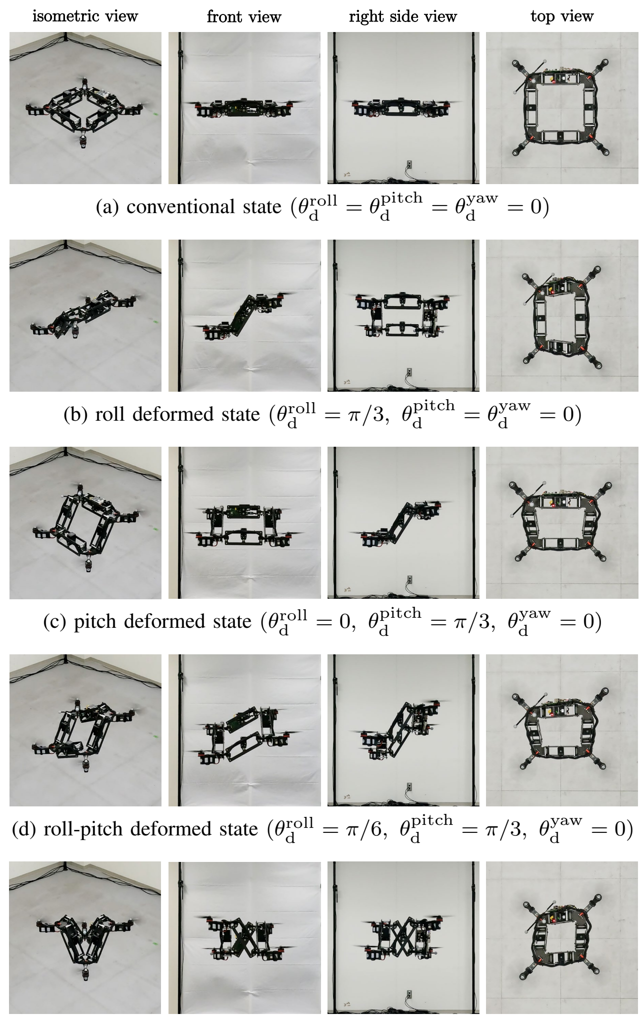

(a) conventional state ($\theta_{\mathrm{d}}^{\mathrm{roll}} = \theta_{\mathrm{d}}^{\mathrm{pitch}} = \theta_{\mathrm{d}}^{\mathrm{yaw}} = 0$)

(b) roll deformed state ($\theta_{\mathrm{d}}^{\mathrm{roll}} = \pi/3,\ \theta_{\mathrm{d}}^{\mathrm{pitch}} = \theta_{\mathrm{d}}^{\mathrm{yaw}} = 0$)

(c) pitch deformed state ($\theta_{\mathrm{d}}^{\mathrm{roll}} = 0,\ \theta_{\mathrm{d}}^{\mathrm{pitch}} = \pi/3,\ \theta_{\mathrm{d}}^{\mathrm{yaw}} = 0$)

(d) roll-pitch deformed state ($\theta_{\mathrm{d}}^{\mathrm{roll}} = \pi/6,\ \theta_{\mathrm{d}}^{\mathrm{pitch}} = \pi/3,\ \theta_{\mathrm{d}}^{\mathrm{yaw}} = 0$)

(e) yaw deformed state ($\theta_{\mathrm{d}}^{\mathrm{roll}} = \theta_{\mathrm{d}}^{\mathrm{pitch}} = 0,\ \theta_{\mathrm{d}}^{\mathrm{yaw}} = \pi/3$)

Fig. 10. Snapshots of the hovering at fixed deformed states.

V. Experiments

The attached video is a summary of this section. An extended version can be found at the following web page: `https://sites.google.com/view/3axis-deformable-frame`.

A. Experimental Platform

In experiments, we use the prototype shown in Fig. 9 in an indoor environment. It has arms 1, 2, 3, 4 and modules 1, 2, 3, 4 made of carbon plates. Following the design method in

TABLE II
RMS ERROR OF THE POSITION AND YAW ANGLE IN HOVERING FOR 60 s AT FIXED DEFORMED STATES SHOWN IN FIG. 10.

Deformed state	p_x [m]	p_y [m]	p_z [m]	ϕ^{yaw} [deg]
(a) conventional	0.0216	0.0246	0.0144	1.084
(b) roll deformed	0.0282	0.0219	0.0201	1.029
(c) pitch deformed	0.0173	0.0208	0.0208	0.949
(d) roll-pitch deformed	0.0233	0.0196	0.0208	0.942
(e) yaw deformed	0.0236	0.0270	0.0222	1.007

TABLE III
FLIGHT TIME OF HOVERING AT DEFORMED STATES SHOWN IN FIG. 10.

Deformed state	t^{hover} [s]
(a) conventional	192
(b) roll deformed	196
(c) pitch deformed	200
(d) roll-pitch deformed	199
(e) yaw deformed	189

Section III, the arm length was determined to be $l_3^{\text{a}} = 54$ mm for the given $l_1^{\text{a}} = 26$ mm, $l_2^{\text{a}} = 40$ mm, and $l^{\text{r}} = 76.2$ mm. From Fig. 7, four identical batteries are distributed on arms 1, 2, 3, 4 for the given $n^{\text{b}} = 4$ with $\boldsymbol{p}^{\Delta} \approx \boldsymbol{0}$ where $\boldsymbol{p}^{\Delta}$ is defined in (12). Therefore, each arm has a rotor with a propeller (`Dalprop TJ6045`), a motor (`Emax RS2205S 2300KV`), and an ESC (`Racerstar RS30A V2`) at the top, and a battery (`Hyperion G8 3S 1400mAh LiPo 30C`) at the bottom. The four batteries are connected in parallel, and their total capacity is 5600 mAh, which gives a hovering flight time of about 195 s. The modules 1, 2, 3 have a servo motor (`Dynamixel XM430-W350-T`) and module 4 has a flight computer (`Holybro Pixhawk4 Mini`) and a companion computer (`Raspberry Pi 4 Model B 8GB RAM`) that are selected to have a low mass ratio $m^{\Delta}/m = 0.57\%$ where $m^{\Delta} = 10$ g and $m = 1.75$ kg.

The host computer acquires the position and yaw angle of the markers fixed on the arm 4 by a motion capture system with 12 cameras (`OptiTrack Prime 13`) using `Motive`, and sends them to the flight computer via the companion computer using `MAVROS`. It also gives the desired values $\boldsymbol{\theta}_{\text{d}}^{\text{rpy}}$, $\boldsymbol{p}_{\text{d}}$, and $\phi_{\text{d}}^{\text{yaw}}$. From the received data, the companion computer gives $\boldsymbol{\theta}_{\text{d}}^{\text{m1,2,3}}$ to daisy-chained three servo motors using `DYNAMIXEL WORKBENCH`, and sends $\boldsymbol{p}^{\text{IMU}}$, $\boldsymbol{p}^{\text{M}}$ to the flight computer using `MAVROS`. The flight computer runs the position controller, attitude controller, and state estimator based on `PX4` [14], [15].

B. Hovering at Fixed Deformed States

First, we performed the hovering experiment at the desired position $\boldsymbol{p}_{\text{d}} = [0\ 0\ 1]^{\top}$ and the desired yaw angle $\phi_{\text{d}}^{\text{yaw}} = 0$ in the fixed states: (a) conventional state $\boldsymbol{\theta}_{\text{d}}^{\text{rpy}} = [0\ 0\ 0]^{\top}$, (b) roll deformed state $\boldsymbol{\theta}_{\text{d}}^{\text{rpy}} = [\pi/3\ 0\ 0]^{\top}$, (c) pitch deformed state $\boldsymbol{\theta}_{\text{d}}^{\text{rpy}} = [0\ \pi/3\ 0]^{\top}$, (d) roll-pitch deformed state $\boldsymbol{\theta}_{\text{d}}^{\text{rpy}} = [\pi/6\ \pi/3\ 0]^{\top}$, and (e) yaw deformed state $\boldsymbol{\theta}_{\text{d}}^{\text{rpy}} = [0\ 0\ \pi/3]^{\top}$. Fig. 10 shows snapshots of the hovering at the fixed deformed states from isometric, front, right side, and top view points. Using the control method in Section IV, the quadrotor was

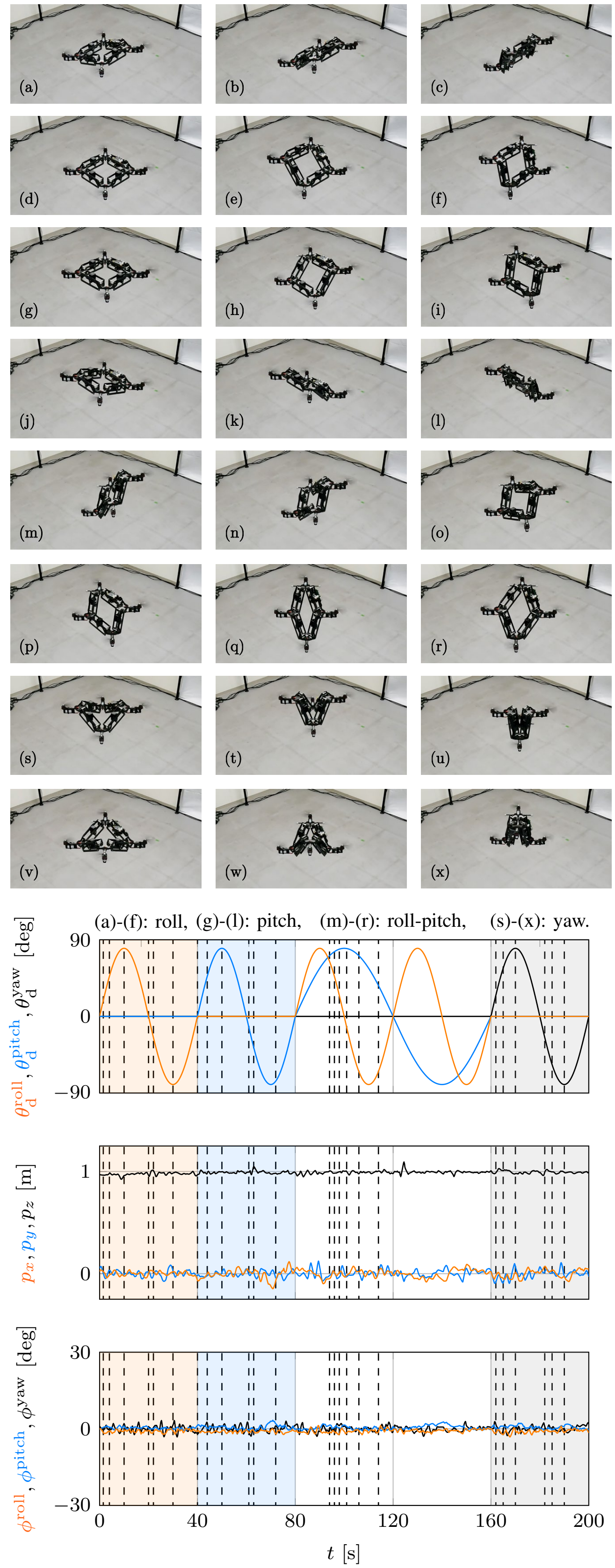

Fig. 11. Hovering with continuous aerial deformations in the roll-only, pitch-only, independent roll-pitch, and yaw directions.

(a) perching

(b) transportation by grasping

Fig. 12. Its applications.

able to fly stably in all states where the gains of the position and attitude controllers were fixed to the adjusted gains at the conventional state. The RMS errors of the position and yaw angle are shown in Table II. The errors do not show a significant dependence on the deformed states. Furthermore, the hovering flight time in each deformed state is shown in Table III. In the table, t^{hover} is the average of the flight time of 5 hovering tests, and there is no significant decrease in t^{hover} due to deformations. This means that the proposed quadrotor can achieve the same hovering efficiency as the conventional one by the design without rotor thrust loss in Section III.

C. Hovering with Continuous Aerial Deformations

Next, we performed the hovering experiment at $\boldsymbol{p}_{\mathrm{d}} = [0\ 0\ 1]^{\top}$ and $\phi_{\mathrm{d}}^{\mathrm{yaw}} = 0$ with continuous aerial deformations: roll-only deformations, pitch-only deformations, independent roll-pitch deformations, and yaw deformations under the same conditions as in Section V-B, that is, the controller gains were fixed. Fig. 11 shows the transient response of the desired deformation parameters $\theta_{\mathrm{d}}^{\mathrm{roll}}, \theta_{\mathrm{d}}^{\mathrm{pitch}}, \theta_{\mathrm{d}}^{\mathrm{yaw}}$, position p_x, p_y, p_z, and attitude $\phi^{\mathrm{roll}}, \phi^{\mathrm{pitch}}, \phi^{\mathrm{yaw}}$ in ZYX Euler angle representation, and snapshots of the deformation transitions. Even with continuous deformations, there are no significant errors in position and attitude, and they converge around the desired values $\boldsymbol{p}_{\mathrm{d}}$ and $\phi_{\mathrm{d}}^{\mathrm{yaw}}$. By using the simple control method that is an extension of the conventional method, it is shown that the quadrotor can be deformed into various shapes in the air.

D. Applications

Finally, we present two applications to demonstrate the advantages of the proposed mechanism. Fig. 12 (a) shows the perching capability. The quadrotor successfully perched on a horizontal cantilever branch in $\mathcal{M}_{\text{roll-pitch}}$ without a perching mechanism [16]. Refer to the web page for perching experiments on a horizontal fixed-end branch and a vertical cantilever branch in $\mathcal{M}_{\mathrm{yaw}}$. Fig. 12 (b) shows the transportation capability in $\mathcal{M}_{\mathrm{yaw}}$. It successfully transported a plastic bottle of mass 0.5 kg by contracting its shape and grasping it without a grasping mechanism [17].

VI. CONCLUSION

In this study, we proposed a novel quadrotor with a frame that can deform in the roll, pitch, and yaw directions using the tilting motions of the parallel link modules. For the quadrotor, we showed a design method without thrust loss due to deformations. In the experiments, we succeeded in hovering at fixed deformed states and in hovering with continuous aerial deformations by using an extended conventional control method. However, the proposed quadrotor may not be stabilized due to the large change of moment of inertia caused by deformations when the onboard batteries are heavy. The future work is to develop a stabilizing controller that depends on the deformation state.

REFERENCES

[1] R. Mahony, V. Kumar, and P. Corke, “Multirotor aerial vehicles: modeling, estimation, and control of quadrotor,” *IEEE Robot. Automat. Mag.*, vol. 19, no. 3, pp. 20–32, 2012.

[2] K. Kawasaki, Y. Motegi, M. Zhao, K. Okada, and M. Inaba, “Dual connected bi-copter with new wall trace locomotion feasibility that can fly at arbitrary tilt angle,” in *Proc. IEEE/RSJ Int. Conf. Intell. Robots Syst.*, pp. 524–531, 2015.

[3] P. Zheng, X. Tan, B. B. Kocer, E. Yang, and M. Kovac, “TiltDrone: a fully-actuated tilting quadrotor platform,” *IEEE Robot. Autom. Lett.*, vol. 5, no. 4, pp. 6845–6852, 2020.

[4] M. Ryll, H. H. Bülthoff, and P. R. Giordano, “A novel overactuated quadrotor unmanned aerial vehicle: modeling, control, and experimental validation,” *IEEE Trans. Control Syst. Technol.*, vol. 23, no. 2, pp. 540–556, 2015.

[5] A. B. Junaid, A. D. D. C. Sanchez, J. B. Bosch, N. Vitzilaios, and Y. Zweiri, “Design and implementation of a dual-axis tilting quadcopter,” *Robotics*, vol. 7, no. 4, pp. 1–20, 2018.

[6] V. Riviere, A. Manecy, and S. Viollet, “Agile robotic fliers: a morphing-based approach,” *Soft Robot.*, vol. 5, no. 5, pp. 541–553, 2018.

[7] A. Desbiez, F. Expert, M. Boyron, J. Diperi, S. Viollet, and F. Ruffier, “X-Morf: a crash-separable quadrotor that morfs its X-geometry in flight,” in *Proc. IEEE Int. Workshop Res., Educ. Develop. Unmanned Aerial Syst.*, pp. 222–227, 2017.

[8] D. Falanga, K. Kleber, S. Mintchev, D. Floreano, and D. Scaramuzza, “The foldable drone: a morphing quadrotor that can squeeze and fly,” *IEEE Robot. Autom. Lett.*, vol. 4, no. 2, pp. 209–216, 2019.

[9] M. Zhao, K. Kawasaki, X. Chen, S. Noda, K. Okada, and M. Inaba, “Whole-body aerial manipulation by transformable multirotor with two-dimensional multilinks,” in *Proc. IEEE Int. Conf. Robot. Autom.*, pp. 5175–5182, 2017.

[10] M. Zhao, T. Anzai, F. Shi, X. Chen, K. Okada, and M. Inaba, “Design, modeling, and control of an aerial robot DRAGON: a dual-rotor-embedded multilink robot with the ability of multi-degree-of-freedom aerial transformation,” *IEEE Robot. Autom. Lett.*, vol. 3, no. 2, pp. 1176–1183, 2018.

[11] A. Sakaguchi, T. Takimoto, and T. Ushio, “A novel quadcopter with a tilting frame using parallel link mechanism,” in *Proc. IEEE Int. Conf. on Unmanned Aircraft Systems*, pp. 666–675, 2019.

[12] T. Fukuda, A. Sakaguchi, T. Takimoto, and T. Ushio, “Modeling and stabilization of the novel quadrotor with tilting propeller,” in *Proc. Symp. Nonlinear Theory Appl.*, pp. 173–176, 2016.

[13] M. Zhao, F. Shi, T. Anzai, K. Okada, and M. Inaba, “Online motion planning for deforming maneuvering and manipulation by multilinked aerial robot based on differential kinematics,” *IEEE Robot. Autom. Lett.*, vol. 5, no. 2, pp. 1602–1609, 2020.

[14] *Controller Diagrams of Autopilot Software PX4*, [Online]. Available: `https://docs.px4.io/master/en/flight_stack/controller_diagrams.html`

[15] L. Meier, D. Honegger, and M. Pollefeys, “PX4: a node-based multithreaded open source robotics framework for deeply embedded platforms,” in *Proc. IEEE Int. Conf. Robot. Autom.*, pp. 6235–6240, 2015.

[16] S. Kirchgeorg and S. Mintchev, “HEDGEHOG: drone perching on tree branches with high-friction origami spines,” *IEEE Robot. Autom. Lett.*, vol. 7, no. 1, pp. 602–609, 2022.

[17] J. Thomas, J. Polin, K. Sreenath, and V. Kumar, “Avian-inspired grasping for quadrotor micro UAVs,” *Proc. Int. Des. Eng. Tech. Conf. Comput. Inf. Eng. Conf.*, 2013.